Thermal diffusivity of isotopically enriched ^{12}C diamond

T. R. Anthony, W. F. Banholzer, and J. F. Fleischer
General Electric Company, Research and Development Center, River Road, Schenectady, New York 12309

Lanhua Wei, P. K. Kuo, R. L. Thomas, and R. W. Pryor
Institute for Manufacturing Research and Department of Physics, Wayne State University, Detroit, Michigan 48202
(Received 27 December 1989)

Type-II *A* diamond single crystals containing approximately 0.1%, 0.5%, and 1% ^{13}C were synthesized and their thermal diffusivities were measured at room temperature by the thermal-wave-mirage technique. The measured value (18.5 cm^2/s) of the 0.1% ^{13}C crystal was 50% higher than the 1% ^{13}C (natural isotope abundance). This is the highest room-temperature thermal diffusivity of any solid naturally occurring or previously synthesized. The laser damage threshold at 193 nm for the isotopically enriched crystal is more than an order of magnitude higher than that of natural diamond.

I. INTRODUCTION

The thermal conductivity of a dielectric solid can be shown by formal transport theory[1] to be

$$K=\tfrac{1}{3}CV\Lambda\ , \tag{1}$$

where C is the specific heat of an assemblage of phonons, V is the speed of the phonons in the solid, and Λ is the phonon mean free path. In a dielectric solid like diamond, C can be taken as the specific heat of diamond and V can be taken as its sound velocity.[2]

The mean free path of phonons in a crystal is a function of many factors. Scattering of phonons can be induced by other phonons, the walls of the crystal, grain boundaries, chemical impurities, vacancies, dislocations, and isotopes. Because very few elements can dissolve in diamond, very pure diamond can be synthesized. Also, grain boundaries can be eliminated and dislocations and wall effects minimized by growing large, high-quality diamond single crystals. The very high binding energy in diamond implies that the vacancy-formation energy is high. Consequently, the equilibrium vacancy concentration is very low in a high-quality diamond crystal that is grown slowly from a liquid melt. Hence, in a large, high-quality diamond single crystal, the phonon scattering that gives rise to thermal resistance is predominantly caused by phonon-phonon and phonon-isotope scattering. With this simplification, the mean free path Λ of phonons may be expressed as

$$1/\Lambda=1/\Lambda_{\text{ph-ph}}+1/\Lambda_i\ , \tag{2}$$

where $\Lambda_{\text{ph-ph}}$ is the mean free path produced by phonon-phonon scattering in diamond and Λ_i is the mean free path generated by phonon scattering by the small amount of the heavy carbon isotope, ^{13}C, in natural diamond (99% ^{12}C and 1% ^{13}C).

Calculations have indicated that, in diamond at room temperature, $\Lambda_{\text{ph-ph}}$ is 30 nm and Λ_i is 2.6×10^3 nm, so that Λ is 30 nm.[1] In other words, the phonon mean free path is reduced by a negligible amount at room temperature as a result of the 1% ^{13}C isotopic "impurity." Other semiempirical correlations[3,4] predict that the thermal-diffusion coefficient enhancement in isotopically pure diamond at room temperature should be less than 5%. However, it should be recognized that a first-principles calculation of the phonon mean free path is difficult, at best, and with that in mind, we have pursued the experimental determination of thermal diffusivity in isotopically enriched diamond, as described below.

II. EXPERIMENT

A. Synthesis of diamond crystals

Isotopically enriched methane (99.9% ^{12}C) was obtained from Cambridge Isotopes Labs of Woburn, Mass., and used to synthesize diamond by means of chemical vapor deposition (CVD) without further purification of the methane. To eliminate sources of ^{13}C contamination from natural carbon impurities in our reactor or in our reactor materials, a new CVD reaction chamber was constructed from materials (quartz and copper) that do not dissolve carbon. The isotopically enriched methane was converted to a sheet of polycrystalline diamond by means of a standard CVD method discussed in the literature.[5–9] X-ray-diffraction, electron-diffraction, and Raman-scattering measurements were used to confirm the identity of the diamond sheet. The Raman peak was centered at 1333 cm^{-1} with a full width at half maximum of 5 cm^{-1}. Previous (unpublished) results showed that the polycrystalline CVD diamond sheet of isotopically enriched diamond had the same thermal conductivity as a similar CVD diamond sheet made from methane with its natural isotopic abundance of carbon.[10]

The isotopically enriched diamond sheet was crushed and powdered and used as a source of carbon for the high-pressure, high-temperature growth of a large single crystal of diamond. Diamond powder must be used as a starting material for growing large highly perfect single

crystals of diamond because of the fact that there is a large volume change in transforming from the graphite to diamond structures. This transformation disturbs the crystal-growing conditions too much to allow the highest-quality crystals to be synthesized. In the present work, a 0.95-carat diamond (sample no. 1) and a 0.92-carat diamond (sample no. 2) of 99.9% ^{12}C were grown from a liquid transition-metal melt at high temperatures and high pressures, using the large-gem temperature-gradient catalyst process invented at the General Electric Research and Development Center.[11,12] The growth of the diamonds was carried out at 52 000 atm and 1200 °C in a belt apparatus capable of sustaining a stable high-pressure and temperature environment for a time sufficient to grow the two crystals. A small single-crystal seed with an orientation of ⟨100⟩ was used to initiate the growth in each case. The transition-metal catalyst was used to ensure formation of a type-II *A* diamond (minimal nitrogen or boron impurities, i.e., the purest known diamond type). The resulting crystals were both clear in color and assessed as "*E*" grade on the standard diamond color scale. The seed crystals were subsequently removed by polishing on a standard diamond scaife. After polishing, the largest ⟨100⟩ face on sample 1 was measured to be 4×7 mm^2 and that on sample 2 measured to be 3.5×4 mm^2.

The small seed crystals contained the natural isotope abundance (1%) of ^{13}C and were the major sources of ^{13}C contamination in the synthesis of samples 1 and 2. Although the seeds were placed at a point in the high-pressure apparatus where they were in contact with a supersaturated solution of carbon in a liquid-metal melt, there remained some danger of carbon exchange between the seed crystal and the solution. This danger of contamination is not as serious as it first appears because of the fact that the seed crystals are themselves 99% ^{12}C and have very small masses (0.005 carats) compared to those of the final crystals. In the worst case, if the seed crystal were to have completely dissolved, the final crystals should contain only 0.005% of the ^{13}C isotope as the result of this contamination.

As an experimental determination of the final isotopic purity of the large single crystal, an analysis was made of sample 1 by Krueger/Geochrom of Cambridge, MA, using a mass-spectroscopic analysis of the combustion products from a piece of the CVD polycrystalline diamond sheet, as well as those from a small parasitic diamond crystal that grew in the same high-pressure cell as did our large diamond. The results of that analysis indicate that the isotopic purity of the polycrystalline CVD diamond sheet and the single-crystal sample 1 were 99.91% and 99.93% ^{12}C, respectively. The slightly higher isotopic purity of the single crystal is not surprising, since growth of a crystal from a liquid can cause some isotopic enrichment as a result of the different atomic jumping frequencies of the ^{12}C and ^{13}C isotopes, both in the solid and liquid phases.

Two other large single crystals of synthetic diamond (samples 3 and 4) were grown in a high-pressure, high-temperature cell using synthetic diamond powder which had been prepared from carbon containing the normal isotopic abundance of 98.96% ^{12}C and 1.04 ^{13}C, and an intermediate-purity crystal (sample 5) was grown with a nominal purity of 99.5% ^{12}C and 0.5% ^{13}C, using the method described above. Finally, a type-II *A* natural gem stone (sample 6) was borrowed[13] and prepared for the thermal measurements in the same fashion as samples 1–5. The preparation procedure is described below.

B. Preparation of diamond crystals for the thermal-wave measurement

The measurement of the thermal diffusivity of a solid by the optical-probe-beam (mirage-effect) detection of thermal waves is simplified if the time-varying energy source of the thermal waves is localized to the surface of the solid. Since diamond is transparent to the modulated argon-ion laser beam used in our experiments, we first prepared the diamond by depositing a thin film on its surface. In carrying out the numerical fits of our theory to the experimental thermal-wave data, we assume that the thermal waves are generated in the film. For our first measurement, carried out on sample 3 (synthetic, type-II *A* natural isotopic abundance), an Ar-F excimer laser, operated at a wavelength of 193 nm and a fluence of 300 mJ/cm^2, was used in this surface preparation. The result of the absorption of the 193-nm (6.4 eV, well above the band edge) radiation was to graphitize a layer (approximately 60 nm thick) on the surface of the diamond crystal. For the isotopically enriched ^{12}C diamond (sample 1), the excimer laser failed to graphitize the diamond surface, even at 10 times the previous fluence. This observation may be due to the much higher thermal diffusivity, which we later confirmed experimentally, or may be the result of changes in the extinction coefficient at 193 nm, or perhaps both factors. Separate spectroscopic measurements are currently underway, the results of which will be reported elsewhere. In order to provide for a reliable surface-absorption layer, therefore, a 100-nm layer of Ti was sputtered from a Ti target over a period of 5 min onto the surface of sample 1, which was held at 350 °C in an Ar atmosphere. This Ti film had a sufficient optical absorption and an adequate adhesion to the diamond crystal for carrying out the optical-probe (mirage-effect) detection of thermal waves, described below. Because of the success of this Ti-film procedure, it was subsequently utilized on all other samples. As a further check on the thermal-wave-diffusivity measurement, a control sample of pure, single-crystal copper was prepared with a nearly identical Ti film on one of its faces.

C. Measurement of thermal diffusivity by the optical-probe (mirage-effect) detection of thermal waves

Our thermal-wave technique for determining the thermal diffusivities of solids has been detailed elsewhere.[14,15] A schematic diagram of our experimental setup is shown in Fig. 1. An argon-ion laser beam is chopped by an acousto-optic modulator at several kilohertz and focused on the surface of the sample to provide a periodic localized surface heat source that generates hemispherical (approximately) thermal waves in the diamond crystal. Thermal waves are also produced in

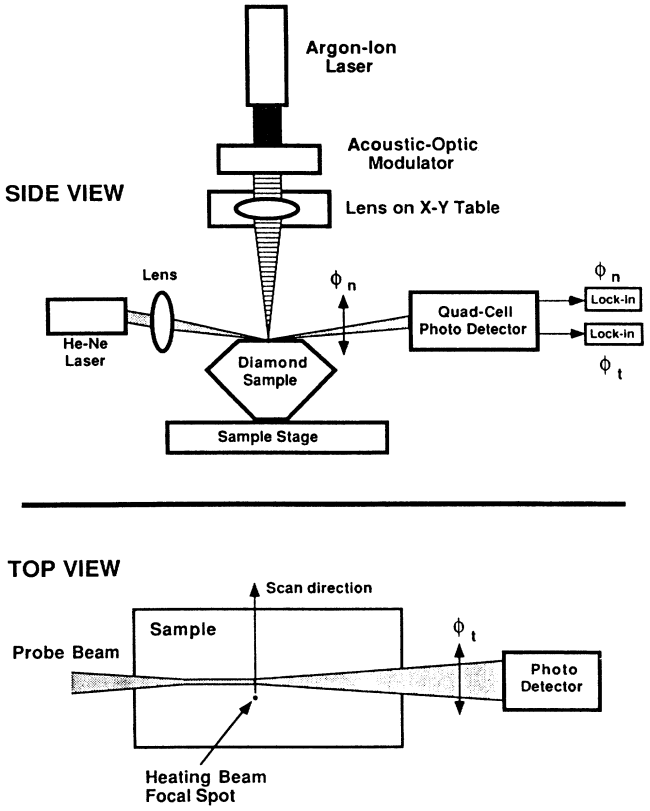

FIG. 1. Block diagram of the optical-probe-beam (mirage-effect) thermal-diffusivity apparatus.

the air that is in contact with the surface of the sample. The presence of the thermal waves in the air is detected by means of a 60-μm-diam He-Ne laser probe beam that bounces at near-grazing angle ($\sim 2°$) from the diamond surface in the vicinity of the focal area of the heating beam. As this beam passes through the heated region of the air, it is refracted by the time-varying gradient in index of refraction of the air (the mirage effect) which accompanies the thermal waves. The magnitude and phase of the vector deflection of this probe beam is then measured by means of a position-sensitive, quad-cell detector, the outputs of which are amplified and fed to two separate vector lock-in amplifiers (one to monitor the vector component of the deflection which is normal to the surface, the other to monitor the transverse deflection). A microcomputer-controlled stepping motor stage is used to move the position of the heating beam across the surface of the sample at right angles to the direction of the probe beam. The two components of the time-varying vector deflection are measured synchronously (magnitude and phase) for each position of the stepping-motor scan, and are recorded in separate memory locations of the microcomputer for later numerical comparison to theory. The scans are repeated for several different frequencies (typically eight), with the computer controlling the entire set of scans, including programmed changes in parameters of the two lock-in amplifiers, and data storage. The resulting data set (typically 12 800 points) is fitted to the theoretical predictions described below, utilizing a multiparameter, least-squares-fitting routine.

It should be pointed out that the measurement is a fundamental one, in the sense that it consists simply of a measurement of length (offset between the two beams) and time (the frequency). No determination of absolute temperature is necessary, only the spatial and temporal distributions of the temperature.

III. THEORY OF MIRAGE SIGNAL FROM A BOUNCED PROBE BEAM

The thermal-diffusion equation in a layered medium with a periodic point source can be solved to give closed-form solutions. For the present experimental situation, a three-layered medium, air/film/substrate, is sufficient. The corresponding transverse, ϕ_t and normal, ϕ_n, mirage signals are given by[15]

$$\phi_{n,t}(x)=\frac{1}{n}\frac{dn}{dT}\int_{-\infty}^{\infty} dk\,\exp(ikx)G_{n,t}(k)\ , \tag{3}$$

with

$$G_n(x)=\frac{q_1}{\kappa_2 q_2\coth\theta+\kappa_1 q_1} \times\exp[q_1 h-k^2 r_1^2/4-(i\omega/\alpha_1)r_2^2/4]\ , \tag{4}$$

and

$$G_t(x)=\frac{ik}{\kappa_2 q_2\coth\theta+\kappa_1 q_1} \times\exp[q_1 h-k^2 r_1^2/4-(i\omega/\alpha_1)r_2^2/4]\ , \tag{5}$$

$$\theta=\tanh^{-1}\left[\frac{\kappa_2 q_2}{\kappa_3 q_3}\right]-q_2 t_2\ , \tag{6}$$

and

$$q_i=(k^2-i\omega/\alpha_i)^{1/2}\ , \tag{7}$$

and where n is the index of refraction of the air, T is the ambient (dc) temperature, ω is the (angular) frequency of modulation, r_1 and r_2 are the radii of the heating and probe beams, respectively, h is the height of the probe beam above the sample surface, x is the offset distance between the heating and probe beams, and α_i and κ_i are the diffusivity and thermal conductance of the ith medium, respectively. The assignments of the suffix are 1, air; 2, film; and 3, substrate.

The above formulas are derived with the assumption that the probe beam skims above the sample surface and penetrates through the ac-temperature field of the heated air and that the entire probe beam is received by the position sensor. This (skimming) method has the drawback that, in order to increase the signal-to-noise ratio, it is necessary to keep the probe beam as close to the heated region as possible. However, that same requirement invariably allows the sample to block part of the skimming probe beam. There is an alternate approach, which we adopt in the present work, in which the probe beam is bounced from the sample surface at or near the heated region.[16] The angle of incidence (measured from the plane

of the surface) is made as small as possible, so that the probe beam is almost parallel to the sample surface. This is referred to as the *bouncing* method to distinguish it from the skimming method. The bouncing method is not without its drawbacks too. For instance, it is applicable only when the sample surface is nearly specular optically. Furthermore, corrections must be made to account for the curvature of the sample caused by the heating (the thermal bump). Fortunately, neither of these considerations is significant for the present experiment. The diamond crystal has a highly polished surface and the reflectivity (with the titanium coating) is over 75%. Also, the thermal-expansion coefficient of diamond at room temperature is extremely small. Thus, the bouncing method is our method of choice for the measurement of diffusivity of diamond crystals. However, the expressions given in Eqs. (4) and (5) must be modified appropriately for this beam geometry. It is necessary to consider separately the mirage effect on the probe beam before and after its reflection from the sample surface, since after reflection the sense of up-down is reversed. When these considerations are incorporated, the expressions for the functions $G_{n,t}(k)$ [Eqs. (4) and (5)] become

$$G_n(x)=\frac{q_1[\mathrm{erfw}(z_2)-\mathrm{erfw}(z_1)]}{\kappa_2 q_2 \coth\theta+\kappa_1 q_1}\exp[(r_1^2+r_2^2)k^2/4]\ , \tag{8}$$

$$G_t(x)=\frac{ik[\mathrm{erfw}(z_2)+\mathrm{erfw}(z_1)]}{\kappa_2 q_2 \coth\theta+\kappa_1 q_1}\exp[(r_1^2+r_2^2)k^2/4]\ , \tag{9}$$

where erfw(z) is a function related to the standard complementary error function by

$$\mathrm{erfw}(z)\equiv\frac{\sqrt{\pi}}{2}\exp(z^2)\mathrm{erfc}(z)\ , \tag{10}$$

with

$$z_{1,2}=\frac{q_1 r_2}{2}\pm\frac{h}{r_2}\ . \tag{11}$$

The expression for θ is unchanged from Eq. (6). Since the probe beam is no longer parallel to the sample surface, the quantity h is redefined as the height of the center of the probe beam where it intersects the heating beam *before* it is reflected from the sample. If it intersects the heating beam *after* it is reflected, it is regarded as negative. The new forms of $G_{n,t}(k)$ indicate that ϕ_t is even and ϕ_n is odd in h.

In the theoretical expressions given above, we have attempted to include most of the effects which contribute to the mirage signal. However, there are a few factors that are either too difficult to account for or are too costly in computation time to be incorporated in the present work. These factors are discussed here as possible sources of systematic errors. The first is the deflection of the probe beam by the thermal bump. It can be reasoned that it contributes primarily to $\phi_n(x)$, because of the near-grazing reflection angle. Furthermore, because of the elastic stiffness of the solid, the bump is expected to spread over a larger range in x than that of the heated region. Thus, its effects are most noticeable for small values of k. We have observed some evidence of this effect in our data. It is most noticeable for the copper data at smaller values of h, where the bouncing point lies closer to the heated region. For the diamond data, its influence is quite negligible. A second possible source of systematic error is the temperature dependence of the diffusivity of air. In addition to the ac-temperature gradient detected by the mirage effect, there is also a dc thermal gradient. Its effect on the deflection of the probe beam is not easily incorporated into the analytic solutions to the diffusion equation. To estimate its influence, we have repeated some of the runs with different heating power, and have seen no significant change in the measured diffusivity of air. A third factor is the local variation in sample surface absorbance. To ensure that the heat source is stable, we operate our heating laser under a optical-power-control mode. Also, the probe-laser power is monitored continuously, and the result is used to normalize the mirage signals. However, any local variation in absorbance can still cause $\phi_n(x)$ and $\phi_t(x)$ to have additional dependences on x. In the present work the Ti coatings have sufficient uniformity to alleviate such concerns. Indeed, the overall quality of the fits in both x space and k space give us confidence that the influence of these factors is not significant.

IV. THE MULTIPARAMETER LEAST-SQUARES-FITTING PROCEDURE

The theoretical expressions above allow one to compare experimentally measured mirage signals in a least-squares-fitting procedure and thereby to deduce values of important physical parameters, such as the thermal diffusivity of the diamond material. Although there are many parameters in these expressions, some of them, such as r_1 and r_2, can be determined by independent experimental measurements. Values of some of the parameters, such as h and t_2, however, are less easily checked.

The nature of a least-squares procedure is that it seeks a local minimum of the squares of the errors in the multidimensional space of the various fitting parameters. Depending on the initital values, which are assumed, the program can be "trapped" at a physically unreasonable local minimum and consequently fail to achieve the true minimum. In fact, there is no foolproof way to determine which of the local minima is the correct one. Nevertheless, we take several measures to guard against such a false minimum. The first precaution is to acquire data for ϕ_t and ϕ_n simultaneously, using two lock-in amplifiers, and then to fit all these data in a single fitting routine, using the same set of parameters. The second measure is to use multiple data sets which are acquired with incrementally different (known) values of experimental parameters (such as frequency), but with identical values of the other experimental parameters, and then once again fit all the data in a single routine with the same set of fitting parameters. Thirdly, we fit the data several different ways, fixing most fitting parameters, while leaving some experimentally known parameters as unknowns in the fitting routine, to be checked against their known values. The

dependence on h is a case in point. The magnitudes of ϕ_t and ϕ_n depend strongly on h, but the *absolute* value of h during a given scan is difficult to determine accurately in an independent measurement. However, several scans can be made in succession with precisely known *differences* of h. When these data are fitted with h simply taken to be a fitting parameter, the agreement between the fitted and experimentally preset *differences* in h is excellent, and gives a very good indication of the integrity of the process.

A typical scan consists of acquring data on both in-phase and quadrature signals of ϕ_t and ϕ_n with two vector lock-in amplifiers for 400 stepped values of x. The expected (or lack of) symmetry properties of $\phi_t(x)$ (odd in x) and $\phi_n(x)$ (even in x) are also used as indicators of the quality of sample surface and beam alignments. The scans are repeated up to eight times with different frequencies and/or heights to comprise a single data set. In our fitting routine, a total of 12 800 data are compared to numerical evaluations of Eqs. (3), (8), and (9) for each iteration of the parameter values, until a best fit is obtained. The forms of ϕ_t and ϕ_n [see Eq. (3)] suggest that the fitting procedure is most efficiently carried out in the Fourier-transform space (k space). The final results are plotted in both x and k spaces (see Sec. V).

V. RESULTS

In order to illustrate the quality of the multiparameter least-squares fits described above, we display four different plots of a typical fit to the 0.07% ^{13}C sample (sample 1) in Figs. 2–5. Figures 2 and 3 show the plots in x space, and Figs. 4 and 5 show them in k space. The curves labeled "x" and "y" in Figs. 5 and 6 represent the in-phase and quadrature components of the signal, respectively. In these plots we have thinned the 400 experimental points per curve for ease of comparison with the theory. It should be noted that the same parameters (including the amplitude and phase) have been used for both ϕ_t and ϕ_n, and for all eight frequencies that have been plotted. The agreement between theory and experiment is excellent, with only small deviations for ϕ_n for values of k less than 0.002 μm^{-1}. A possible cause for these slight deviations has been discussed in Sec. III. It should also be noted that the significant changes in both slope and curvature of the k-space curves are faithfully borne out by the data (see Figs. 4 and 5, and especially the "y" curves for 4 and 10 kHz). We have achieved similarly ex-

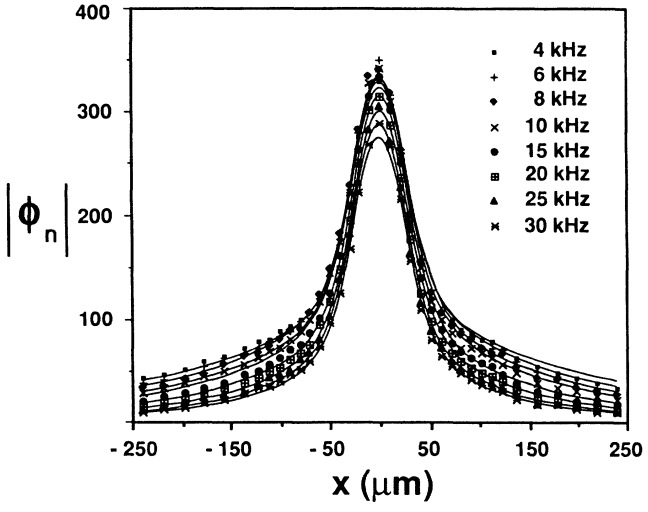

FIG. 2. Magnitude of the normal component of the mirage signal as a function of the offset distance between the heating and probe beams for eight different frequencies in sample 1 (99.93% ^{12}C). Experimental points are represented by symbols and theoretical values by lines.

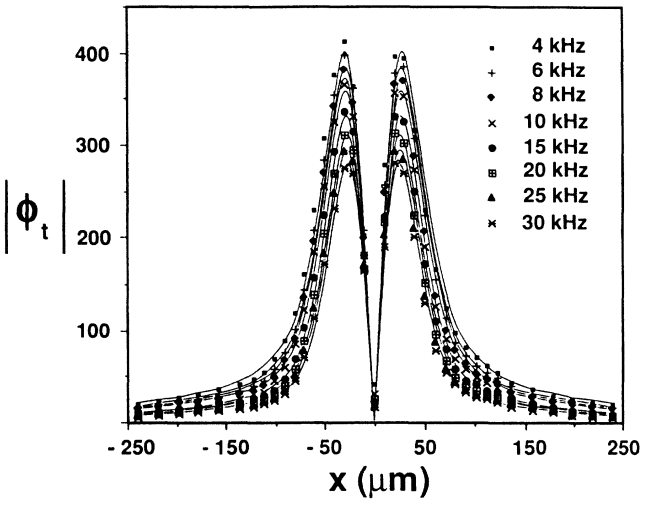

FIG. 3. Magnitude of the transverse component of the mirage signal as a function of the offset distance between the heating and probe beams for eight different frequencies in sample 1 (99.93% ^{12}C). Experimental points are represented by symbols and theoretical values by lines.

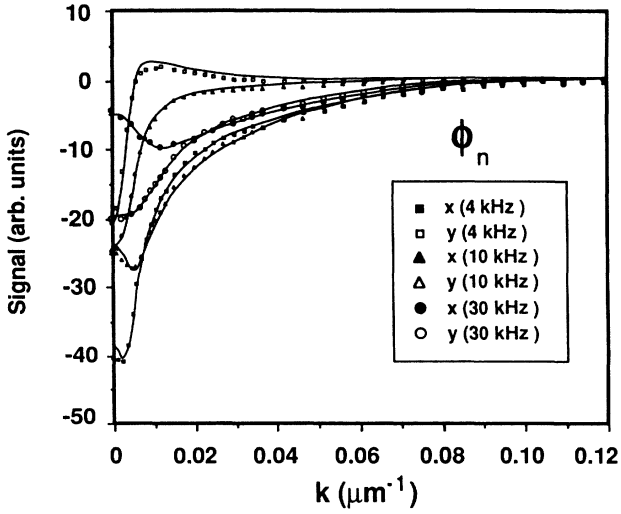

FIG. 4. In-phase x and quadrature y components of the Fourier transform of Fig. 2 for three different frequencies.

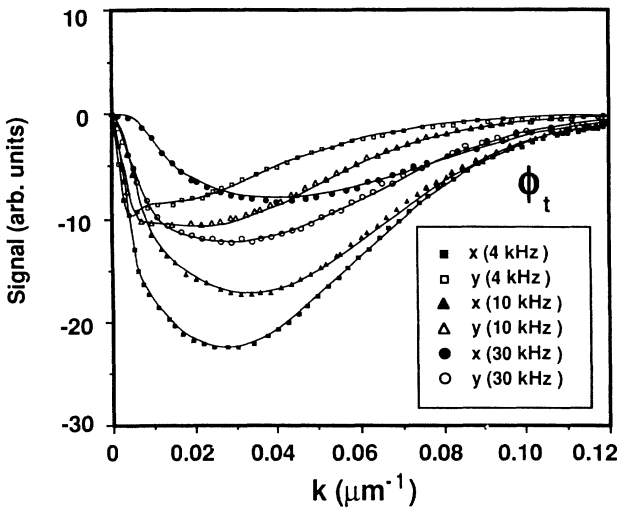

FIG. 5. In-phase x and quadrature y components of the Fourier transform of Fig. 3 for three different frequencies.

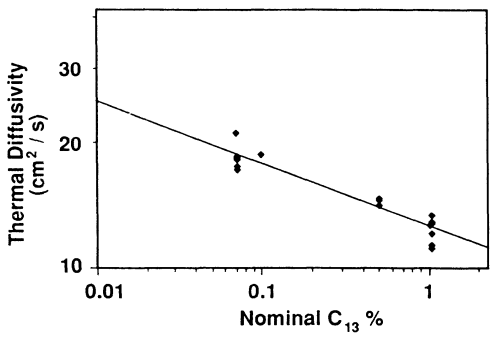

FIG. 6. Summary (log-log) plot of the thermal diffusivities of the diamond samples tabulated in Table I.

cellent quality of fits for all of our diamond data. As discussed in Sec. III, the fits for our Cu data are slightly poorer, but with a resulting diffusivity which is in excellent agreement with values found in the literature. Furthermore, our fits for Cu data collected on a surface

TABLE I. Summary of experimentally measured thermal diffusivities for the five synthetic and one natural type-II A diamond crystals, together with the measured values for a pure single-crystal Cu control sample. Also tabulated are the experimental run parameters.

Sample no.	Nominal ^{13}C (%)	Coating	Orientation[a]	No. of frequencies	No. of heights	Diffusivity (cm^2/s)	Variance
1	0.07	Ti (1000 Å)	large (100)	8	1	18.5	0.0026
1	0.07	Ti (1000 Å)	large (100)	8	1	18.6	0.0014
1	0.07	Ti (1000 Å)	large (100)	1	5	18.6	0.0032
1	0.07	Ti (1000 Å)	large (100)	8	1	18.6	0.0016
1	0.07	Ti (1000 Å)	large (100)	8	1	18.4	0.0010
1	0.07	Ti (1000 Å)	large (100)	8	1	18.3	0.0010
1	0.07	Ti (1000 Å)	1 (111)	8	1	18.5	0.0011
1	0.07	Ti (1000 Å)	2 (111)	8	1	17.2	0.0011
1	0.07	Ti (1000 Å)	2 (111)	5	1	18.3	0.0008
1	0.07	Ti (1000 Å)	2 (111)	8	1	18.6	0.0009
1	0.07	Ti (1000 Å)	1 (111)	8	1	21.2	0.0014
1	0.07	Ti (1000 Å)	1 (111)	8	1	17.2	0.0012
1	0.07	Ti (1000 Å)	1 (111)	8	1	17.6	0.0014
2	0.1	Ti (1000 Å)	1 (111)	8	1	18.8	0.0009
3	1.04	graphite (600 Å)	large (100)	5	1	11.2	0.0034
3	1.04	graphite (600 Å)	large (100)	5	2	11.4	0.0049
3	1.04	graphite (600 Å)	large (100)	5	1	12.1	0.0041
3	1.04	Ti (1000 Å)	large (100)	8	1	12.9	0.0023
3	1.04	Ti (1000 Å)	large (100)	8	1	12.8	0.0011
3	1.04	Ti (1000 Å)	large (100)	8	1	13.5	0.0006
3	1.04	Ti (1000 Å)	large (100)	8	1	12.9	0.0010
4	1	Ti (1000 Å)	large (100)	8	1	12.7	0.0030
5	0.5	Ti (1000 Å)	1 (111)	8	1	14.6	0.0012
5	0.5	Ti (1000 Å)	1 (111)	8	1	14.7	0.0012
5	0.5	Ti (1000 Å)	3 (111)	8	1	14.2	0.0010
6	natural II A	Ti (1000 Å)	large (100)	8	1	12.2	0.0008
Cu		no coating		3	1	1.3	0.0010
Cu		no coating		3	1	1.3	0.0021
Cu		no coating		3	1	1.2	0.0015
Cu		Ti (1000 Å)		5	1	1.25	0.0010

[a] 1, 2, or 3 refers to facet no.

covered by a Ti film give the same diffusivity as do our fits on an uncoated Cu surface.

A summary of all the results of our diamond thermal-diffusivity measurements is given in Table I. The column labeled "variance" in Table I is a measure of the quality of the multiparameter fit, and is simply the statistical variance between the theory and the typically 12 800 values of experimental data. Our thermal-diffusivity result (12.4 ± 1 cm^2/s) for synthetic samples having the natural isotopic abundance is in good agreement with values calculated from handbook values of thermal conductivity and heat capacity.[17] Our result for the natural crystal (12.2 ± 1 cm^2/s) is in similarly good agreement. Our measured values (18.5 ± 1 cm^2/s) for the 99.9% isotopically enriched samples are indicative of a 50% enhancement in thermal diffusivity. Our measured value (14.5 ± 1 cm^2/s) for the intermediate-isotopic-purity (99.5%) sample is consistent with the other results. A summary (log-log) plot of all the diamond diffusivity values from Table I is given in Fig. 6. A naive extrapolation of this plot to ^{13}C concentrations of the order of 0.01% could result in a 100% enhancement in room-temperature diffusivity from that of high-quality natural diamond. In summary, our 99.9% ^{12}C- enriched crystals have the highest room-temperature thermal diffusivity (18.5 ± 1 cm^2/s) of any solid naturally occurring or previously synthesized.

VI. DISCUSSION

If we assume that the specific-heat capacity and the density of the enriched samples do not differ significantly from their values for samples with the natural isotopic carbon abundance, then we can calculate values of thermal conductivity corresponding to the diffusivity values tabulated in Table I by using the definition $\alpha=\kappa/\rho C$, where α is the thermal diffusivity, ρ is the mass density, and C is the specific-heat capacity. This results in a conversion factor at 25 °C of $\kappa=(1.795\pm0.032)\alpha$. The thermal conductivity of the isotopically enriched 99.9% ^{12}C type-II A diamond is then found to be 33 ± 2 W cm^{-1} K^{-1}. A comparison of the thermal conductivities of these crystals with other substances[2,4] is given in Table II.

TABLE II. Comparative thermal-conductivity values from this work and selected earlier studies on high-conductivity materials.

Material	Thermal diffusivity (cm^2 s^{-1})	Thermal conductivity (W cm^{-1} K^{-1})
0.07% ^{13}C diamond (this work, enriched)	18.5	33.2
0.5% ^{13}C diamond (this work, enriched)	14.5	26.0
1.0% ^{13}C diamond (this work, natural abundance)	12.4	22.3
natural diamond (this work, Ref. 2)	12.2	21.9
CVD diamond (Refs. 5–9)		12.0
cubic boron nitride (Ref. 4)		7.6
silicon carbide (Ref. 4)		4.9
copper (Ref. 4)	1.25	4.0
beryllium oxide (Ref. 4)		3.7
boron phosphide (Ref. 4)		3.6
aluminum nitride (Ref. 4)		3.2
silicon (Ref. 4)	0.86	1.6
aluminum oxide (Ref. 4)		0.2

VII. SUMMARY

High-quality diamond crystals were synthesized, respectively, from diamond feed stock having three different isotopic distributions of carbon. Heuristic arguments predict that the thermal conductivity of the isotopically pure diamond should increase, at most, by about 5% at room temperature because of a reduction in phonon-isotope scattering. Experimentally, we have found an increase of 50% in the diffusivity, implying a corresponding decrease in the phonon-isotope scattering if one assumes that C and V are comparatively unaffected by the isotopic impurities. We have also observed that the damage threshold at 193 nm for the isotopically enriched crystal is substantially higher than that for the crystal with the natural isotopic mix. These ^{12}C-enriched crystals consequently have the highest room-temperature thermal conductivity of any solid naturally occurring or previously synthesized. A naive extrapolation of our experimental results to purer ^{12}C diamond indicates a potential enhancement of room-temperature thermal conductivity of over 100%.

ACKNOWLEDGMENTS

The authors would like to thank W. L. Robb, A. S. Hay, W. E. Smith, and M. M. O'Mara for their interest and support of this work, and J. W. Bray and G. A. Slack for some stimulating discussions, and Dubbeldee Diamond of Drukker, and K. Harris and M. Seal for providing a natural type-II A diamond. The thermal-diffusivity measurements were partly sponsored by the Institute for Manufacturing Research, and by The Army Research Office, U.S. Department of Defense under Contract No. DAAL03-88-K-0089. The authors would like to thank G. Reck and K. Borst for assistance in sample preparation.

[1]J. M. Ziman, *Electrons and Phonons* (Oxford University Press, London, 1963).

[2]J. E. Fields, *The Properties of Diamond* (Academic, London, 1979).

[3]G. A. Slack, Phys. Rev. **105**, 829 (1957).

[4]G. A. Slack, R. A. Tanzilli, R. O. Pohl, and J. W. VanderSande, General Electric Co. Technical Information Series Report No. 84CRD126, 1984 (unpublished).

[5]Benno Lux and Roland Haubner, in Proceedings of the 12th International Plansee Seminar, 1989 (unpublished), p. 615.

[6]R. C. Devries, Annu. Rev. Mater. Sci. **17**, 161 (1987).
[7]K. E. Spear, J. Am. Ceram. Soc. **72**, 171 (1989).
[8]J. C. Angus and C. C. Hayman, Science **241**, 913 (1988).
[9]P. K. Bachman and R. Messier, Chem. Eng. News **67**, 24 (1989).
[10]T. R. Anthony, J. F. Fleischer, D. Cahill and J. Olsen (unpublished).
[11]R. H. Wentorf, J. Phys. Chem. **75**, 1833 (1971).
[12]G. S. Woods and A. R. Lang, J. Cryst. Growth **28**, 215 (1975).
[13]Dubbeldee Harris Diamond Corporation, Mount Arlington, NJ.
[14]L. D. Favro, P. K. Kuo, and R. L. Thomas, in *Photoacoustic and Thermal Wave Phenomena in Semiconductors,* edited by A. Mandelis (Elsevier, New York, 1987), Chap. 4, pp. 69–96.
[15]P. K. Kuo, L. D. Favro, and R. L. Thomas, in *Photothermal Investigations of Solids and Fluids,* edited by J. A. Sell (Academic, New York, 1988), Chap. 6, pp. 191–212.
[16]C. B. Reyes, J. Jaarinen, L. D. Favro, P. K. Kuo, and R. L. Thomas, in *Review of Progress in Quantitative Nondestructive Evaluation,* edited D. O. Thompson and D. E. Chimenti (Plenum, New York, 1987), Vol. 6, pp. 271–275.
[17]*CRC Handbook of Chemistry and Physics,* 67th ed., edited by Robert C. Weast (Chemical Rubber Co., Cleveland, 1986), pp. B82, D58, D178, and E11.

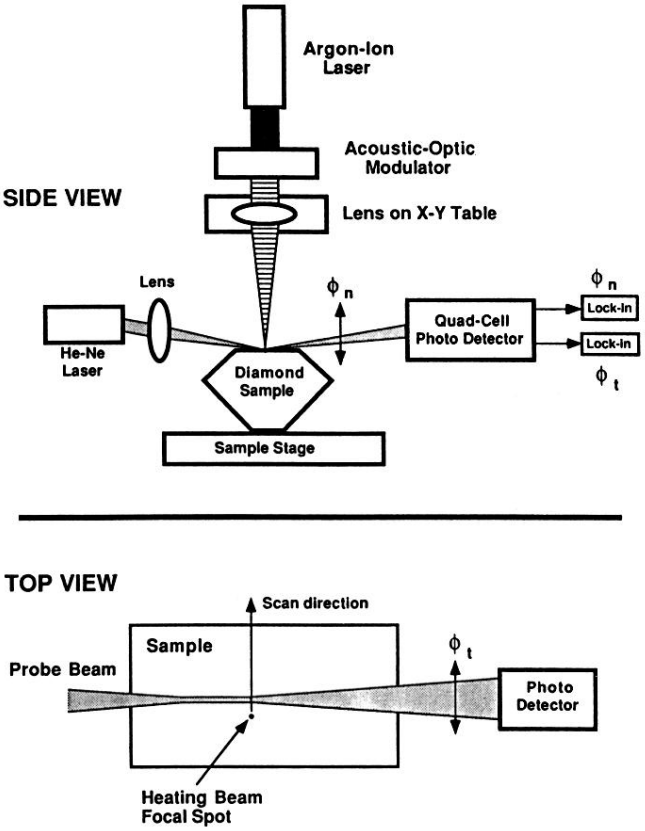

FIG. 1. Block diagram of the optical-probe-beam (mirage-effect) thermal-diffusivity apparatus.